NASA TECHNICAL MEMORANDUM

NASA TM X- 68283

NASA TM X- 68283

A VISUAL STUDY OF RADIAL INWARD CHOKED FLOW OF LIQUID NITROGEN

by R. C. Hendricks, R. J. Simoneau, and Y. Y. Hsu
Lewis Research Center
Cleveland, Ohio 44135

TECHNICAL PAPER proposed for presentation at
Cryogenic Engineering Conference
Atlanta, Georgia, August 8-10, 1973

Page Intentionally Left Blank

A VISUAL STUDY OF RADIAL INWARD CHOKED FLOW OF LIQUID NITROGEN

by R. C. Hendricks, R. J. Simoneau, Y. Y. Hsu

Lewis Research Center

E-7605

ABSTRACT

Data and high speed movies were acquired on pressurized subcooled liquid nitrogen flowing radially inward through a 0.0076 cm (3 mil) gap. The stagnation pressure ranged from 0.7 to 4 MN/m^2 ($0.2 \leq P/P_c \leq 1.2$). The results of this qualitative study indicate:

1. Steady radial inward choked flow appears equivalent to steady choked flow through axisymmetric nozzles.

2. Transient choked flows through the radial gap are not uniform and the discharge pattern appears as nonuniform impinging jets.

3. The critical mass flow rate data for the transient case appear different from those for the steady case. On the mass flow rate vs pressure map, the slope and separation of the isotherms appear to be less for transient than for steady radial choked flow.

SYMBOL LIST

A	area, cm^2
D	hydraulic diameter, cm
G	mass flux, g/cm^2-sec
G_R	reduced mass flux
$G^*=\sqrt{\rho_c P_c/Z_c}$	mass flux normalizing constant g/cm^2-sec. For nitrogen $G^*=6010$.
L	passage length, cm
M	mass, g
P	pressure MN/m^2 (psia)

$P_R=P/P_c$	reduced pressure
T	temperature, K
$T_R=T/T_c$	reduced temperature
V	volume, cm^3
y	vertical distance, cm
$Z=P/\rho RT$	compressibility factor
Δ	difference
ρ	density, g/cm^3
τ	time, sec

Subscripts

bulk	bulk
c	critical
o	stagnation
sat	saturation
R	reduced

INTRODUCTION

Choked flows are common in gas lubricated bearings, seals, and in the venting of high energy systems when they "go critical." However, little is known about using a vaporizing liquid as a seal or in bearings, or leaks through cracks in either the transient or steady state cases.

The motivating problem of interest is to be able to predict the leak rate and possible onset of two-phase flow instability due to maldistribution of pressurized cryogens discharging into space through a long narrow rotating passage with heat being added along the walls and/or generated by the fluid.

Some of the unique features of the problem are: the small gap heights required (0.0008-0.0013 cm), L/D values of (100-200), and a flow aspect ratio (passage front/passage

height) of order 10^4. These parameters could result in maldistribution of vapor and liquid flow, surface capillary effects, thermodynamic nonequilibrium, boiling and vapor entrainment, etc. While the efforts of several researchers have been directed at two-phase choked flows (refs. 1, 2, 3, and 4). Little or no research has been done on these questions within the above range of parameters.

A quantitative study was undertaken to delineate some of the problems associated with radial inward flow through a narrow stationary gap which chokes and discharges through a central pipe. The data and accompanying high speed movie were taken to explore the problems.

APPARATUS

The basic apparatus used in this study is illustrated in figure 1. Pressurized liquid nitrogen flowed through the radial gap and out of the cryostat. In this study, the radial flow passage was formed by a glass cover separated from the stainless steel orifice by three radial wires 0.0076 cm diameter (3 mil). Details of the radial gap-nozzle are given on figure 1.

A 10-common-wire Chromel-Alumel thermocouple rake was constructed to monitor the liquid level in the reservoir. The rake frame was made of bakelite and the thermocouple junctions were made at 0.63 cm (1/4 in.) intervals from the face of the bakelite insert.

The reservoir temperature was monitored by a platinum thermometer, located 0.95 cm (3/8 in.) above the radial gap. A second platinum thermometer near the top of the thermocouple rake was used as a check under no flow conditions.

The vacuum jacket was usually not better than 500μ, however some of the heat leak was offset by the evaporated nitrogen which leaked past the window seals.

STEADY-STATE RESULTS

In order to obtain steady-state critical flow data, the entire apparatus of figure 1 was mounted in the blowdown facility (fig. 2) with a reservoir capacity of 120 liters which is quite sufficient for all steady flows taken in this study. The entire system could be precooled from ambient temperature down to about 80K, which enabled us to achieve

various reduced temperatures starting at $T_R = 0.7$. Since the blowdown facility was sized for an order of magnitude larger flow area, the extremely low mass flows could not be metered to a certainty greater than 5 percent; however, for gaseous flows the two flowmeters agreed within 3 percent. Peculiar temperature inversions were often noted in the flows from the reservoir of figure 2 into the apparatus of figure 1. These may have been due to tank stratification, coupled with gas residual in the apparatus. For all the data reported herein, the flowmeter between the reservoir and the apparatus was used.

The critical mass flow rates for several fluids can be correlated using the principle of corresponding states, reference 4. The flow rate normalizing parameter

$$G^* = (\rho_c P_c / Z_c)^{1/2}$$

reference 4, is used to normalize the flow data presented herein. The gaseous data, figure 3 and table I, appear to be in reasonable agreement with previously determined data for gaseous flow through nozzles. This, of course, gives us a certain degree of confidence in our results. The trends in the data for the $T_R = 0.8$ isotherm are very similar to those of the axisymmetric nozzle data (refs. 3 and 4). Solid lines on figure 3 are used to represent the data of reference 4. Data trends for other isotherms are in equally good agreement, as can be noted in figure 3. One questionable area appears to be the $T_R = 1.035$ isotherm near $P_R = 1.2$. These data are presented in table I.

The general agreement between the data of table I and that of references 3 and 4 indicate that there is little difference in the critical flow phenomenon between the axisymmetric nozzle and radial inward flow through a 0.0076 cm (3 mil) gap having an outer to inner area ratio of ~ 13:4, see figure 1. This is quite significant as the geometries are very different and tends to imply the generality or the usefulness in the application of the technique of reference 4 to odd geometries.

TRANSIENT RESULTS

Because of the uncertainties in determining the parameters which make up critical flow rate, i.e. density, area, and volumetric flow rate, exact values of G were not determined. However some interpretations of the data were made and are

presented in the appendix. In essence, two techniques are used to predict transient data with limited success. The transient results depart in both slope and level when compared to the steady state results. Further investigation of the disparities are required.

PHOTOGRAPHIC SEQUENCES

Transient Conditions

Motion pictures were taken at 100, 400, 5000, and 16 200 frames per second to provide greater detail to flow patterns and the gas-liquid interface within the reservoir. For all tests, the back pressure is near ambient and the fluid is nitrogen.

$$P_{critical} = 3.417 \text{ MN/m}^2 \text{ (33.72 atm)};$$

$$T_{critical} = 126.3 \text{ K};$$

$$\rho_{critical} = 0.3105 \text{ gm/cc}.$$

During the flow transient, the ullage space is continually charged with high pressure nitrogen gas at ambient temperature. The charge rate is not sufficient to maintain constant pressure but does provide adequate isobaric subcooling, i.e.

$$(T_{sat} - T_{bulk}) > 0.$$

The combination of decreasing pressure with increasing temperature provides a spectrum of flow regimes from subcooled, to saturated, to gas-droplet entrainment.

In general the flow patterns are irregular and the flow area covered by the single phase fluid is much greater than the area where two-phase phenomena occur.

Description of Setup

Sequences to illustrate the behavior of the gas-liquid interface during transient flow were taken at 100 frames per second. The camera viewed the interface through the side windows of the cryostat, and the apparatus is as illustrated

in figure 1. The thermocouple rake, platinum thermometers, glass cover plate as well as reservoir thermals are clearly illustrated. These sequences could not be taken simultaneously with those viewed from the top.

To obtain more definitive pictures of radial inward choked flow as viewed from the top and raise the liquid level, the single 3/8 in.-thick glass cover plate of figure 1 was replaced by a stack of three 3/8 in.-thick glass plates, and the camera speed increased to 400 frames per second. The pictures were taken while maintaining the upper portion of the tank, namely the camera viewing window, above the condensation temperature, and filling the dewar only to the level of the stacked glass plates. Previous experience indicated that ullage gas would condense on the window and other parts of the dewar, form liquid drops and/or rivulets which obscured direct observation.

In the quest for more definition, top-viewed sequences were taken with top and side lighting at an effective camera speed of 16 200 frames per second with an equivalent shutter speed of 152 000 frames per second. This was achieved by running the camera at 8100 frames per second and recording an 8 mm split frame image as viewed through a narrow slit. At these speeds the entrainment of voids can be studied but camera speed of another order of magnitude is required to study the choking interface.

Description of Film Sequences

Film Sequence 1

To illustrate the flow patterns in subcooled-subcritical-nitrogen the stagnation pressure and temperature in the cryostat is set at 0.79 MN/m^2 (114.2 psia) and 87.1 K respectively which represents a subcooling of 13 K. At the opening of the valve, the fluid surface vibrates and a white central two-phase region begins to form. Note that the flow discharges as an array of nonuniform jets. The flow patterns are not stable and the jets extend inward far beyond the nozzle edge, the minimum area, where choking should occur. Such behavior indicates a substantial degree of nonequilibrium. The average pressure during discharge is 0.75 MN/m^2 (109 psia) with a depressurization rate of -0.0035 MN/m^2-sec (-0.5 psia/sec). While the gas-liquid interface remains quite calm, thermals as well as flow patterns of the fluid approaching the nozzle can be seen. At the reduced liquid levels, the temperature of

the fluid entering the nozzle approaches saturation and the jet sources begin to extend outward. The effects of small surface defects (pits or sites) can be noted in addition to the nonuniformity of the two-phase front. Further reduction in the level permits the visualization of strong surface tension effects, the entrainment of gas and a rapid development of a fan pattern which finally fills the radial gap-nozzle.

Figure 4(a) represents this film sequence.

Film Sequence 2

In direct contrast to the subcritical pressure patterns of Film Sequence 1 this sequence represents fluid nitrogen in its supercritical pressure state. The stagnation pressure and temperature are 4.2 MN/m^2 (609.2 psia) and 121.8 K respectively. Here the transposed critical temperature* is 130.7 K, so the fluid is in a sense subcooled nearly 9 K. At the opening of the valve, the central two-phase region (white) develops rapidly. The region is not steady nor does it have periodic oscillations and distinct jetting is difficult to determine. The average pressure during discharge is 4.0 MN/m^2 (579 psia) with a depressurization rate of -0.47 MN/m^2-sec (-68 psia/sec) during the initial phase of the transient and -0.096 MN/m^2-sec (-13.9 psia/sec) during the major portion of the discharge cycle. A view of the gas-fluid interface reveals the formation of a "milky" layer approximately 1 cm thick. By carefully following the procedure described in Description of Setup, the thickness of this layer was minimized and pictures of the flow patterns were obtained.

Figure 4(b) represents this film sequence. As the run progresses, the reservoir pressure decreases and the liquid temperature increases due to heat transfer through the ullage gas from the make up gas. At the beginning of the fan pattern the pressure is 3.86 MN/m^2 (545.2 psia) and the temperature measured at the platinum thermometer level which is 0.95 cm (3/8 in.) above the radial flow plane is 129.1 K. This temperature is characteristic of the mixed gas-condensate interface

*The transposed critical temperature is a point corresponding to a sharp peak in specific heat, C_p. It is a function of pressure. At this temperature the density changes rapidly from high to low density. In a sense it can be thought of as a "supercritical saturation temperature equivalent."

and the fan patterns which follow are presumed to be "mist flow." Note the multiplicity of variations in the choking front as temperature increases and pressure decreases. The appearance of inner and outer ring patterns suggest that two fronts exist in the nozzle. At least the picture suggests multiple regions with large gradients.

Sequence 3

During the course of a run at the 4 MN/m^2 pressure level, a nonhomogenity which looked like a bubble was entrained into the nozzle. The reduced pressure and temperature are approximately 1.2 and 0.96 respectively. Bubbles should not form under these conditions. The picture sequence is expanded in order to view the nonhomogenity.

Sequence 4

To illustrate flow patterns near the thermodynamic critical point, the initial pressure is 3.48 MN/m^2 (506.2 psia) and the temperature is 126.9 K. These conditions are just above the thermodynamic critical point. The temperature is quite close to the transposed critical temperature of 127 K, consequently the "subcooling" is smaller than the previous sequence. Note the aperiodic oscillations of the two-phase region which appears white. Further note that on an area basis, most of the flow field within the nozzle appears nonoscillatory and homogeneous. The average pressure during discharge is 3.3 MN/m^2 (480 psia) with an initial depressurization rate of -0.38 MN/m^2-sec (-54.5 psia/sec) and average of -0.092 MN/m^2-sec (-13.4 psia/sec). As the reservoir empties the fan pattern is observed. The pressure has decreased to 3.26 MN/m^2 (472.2 psia) which is less than critical pressure while the temperature has increased to 127.8 K at the platinum thermometer, 0.95 cm above the nozzle plane. The mist flow regimes become apparent, even though the conditions are quite close to the critical point.

Sequence 5

In the following three sequences the flow patterns are illustrated for three selected subcooled-subcritical pressures. At the opening of the valve the pressure is 2.82 MN (409.2 psia) and the temperature is 113.6 K. This represents a subcooling of 9.4 K. This level of subcooling persists over most of the film sequence, however at the development of the fan

pattern the temperature is within ±1 K of the saturation temperature. The average pressure is 2.7 MN/m^2 (384 psia) with an initial depressurization rate of -0.22 MN/m^2-sec (-32.5 psia/sec) and an average rate of -0.045 MN/m^2-sec (-6.5 psia/sec). The oscillations of the two-phase region become more apparent and the choking front begins to extend outward, however the majority of the nozzle is still in homogeneous nonoscillating flow. At the onset of the fan pattern evidence of an interface or surface tension effects on the entrained flow can be detected.

As time progresses, the entrained mist flow transitions to high density vapor flow.

Sequence 6

As the valve opens the pressure is 2.16 MN/m^2 (313.2 psia) and the temperature is 96.8 K. This represents a subcooling of 10.2 K. As the flow rate has diminished considerably, the pressure-temperature-time profiles are nearly linear. The average pressure is 2 MN/m^2 (294 psia) and the depressurization rate is -0.037 MN/m^2-sec (-5.3 psia/sec). Oscillation in the two-phase region is commonplace and the nonuniform two-phase front has extended in an erratic manner into the nozzle. Most of the nozzle on an area basis is still in uniform flow. As the radial fans appear, the effects of surface tension are now easily observed. The pressure has decreased to 1.95 MN/m^2 (283.2 psia) and the temperature at the platinum thermometer above the nozzle plane is 117.5 K. Again the nozzle flow transitions through several flow regimes from subcooled saturation, super saturation, mist flow and finally cold vapor. Within these latter frames one can visualize what the nozzle flow would look like if it were flowing--steady state--in each of these regimes; furthermore the picture sequence illustrates the transition boundaries between these states. Peripheral waviness noted in the pictures is due to light reflections from the interface and does not represent nozzle characteristics.

Sequence 7

At 1.5 MN/m^2 (217.2 psia) and 94.3 K the reservoir is subcooled 5.9 K. As the valve opens, the development of the choking region is observed. The average pressure is 1.4 MN/m^2 (205 psia) with a depressurization rate of -0.0147 MN/m^2-sec (-2.12 psia/sec). The two-phase region is oscillatory in

nature and the front extends erratically into the nozzle. While most of the nozzle appears homogeneous, the erratic two-phase radial spikes seem to make the uniform circular two-phase choking front model a mathematical concept whose usefulness is fortuitous. The time temperature-pressure profiles are quite linear and diminish to 1.39 MN/m^2 (201.2 psia) and 109 K at the platinum above the nozzle plane as the fan patterns begin. The effects of surface tension are clear and appear to exert considerable forces on the flow field. The nozzle is clearly not in equilibrium and combinations of droplets, cold vapor and liquid are seen to coexist within various sections.

Sequence 8

To illustrate the flow characteristics of a saturated fluid, the 1.5 MN/m^2 pressure was chosen because of its relation to a seals project at Lewis Research Center. To view the phenomena more clearly the frame rate was changed to about 5000 frames per second and the nozzle lighted from the top and the side. Note the extreme irregularity of the interface which is delineated by the two-phase streaks toward the nozzle center. It would seem that the two-phase choking interface per se does not exist but rather a highly nonequilibrium nonsteady transition between liquid and vapor. As bubbles are ingested, large vapor rays separate the liquid and plunge into the orifice exit.

Sequence 9

In order to study these bubble streaks better, the frame rate is increased to 8100 8 mm-split frame images per second, equivalent to 16 200 frames/sec. One can now see that bubbles are elongated as they approach the entrance of the nozzle and are sucked through. The leader seems to be spherical and nonsteady, but progresses in a linear manner to the "interface" or choked front. In this stop frame sequence one can see the advance of a bubble about 30° off the bottom of the picture (counter-clockwise) and shortly after this bubble is halfway across the nozzle a second bubble enters at 10° (clockwise) from the bottom. The vapor streamers persist for quite some time before the gap is closed.

Figure 4(c) represents this film sequence.

Sequence 10

To illustrate the influence of surface pits and scratches, we see here the activation of a site about 30° counter-clockwise from the bottom and midway across the nozzle. The camera speed is 16 200 frames per second.

SUMMARY-MOTION PICTURES

In summary, motion pictures have been taken which illustrate several aspects of radial inward choked flow of fluid nitrogen.

Sequence 11

This split frame sequence compares radial inward choked flow at supercritical and subcritical pressures. The reduced pressures are approximately $P_R = 1.17$ and $P_R = 0.22$ respectively. It does appear that the flow field is more homogeneous for $P_R > 1$; because of its erratic nature the "choking" interface appears larger for $P_R < 1$. Both flow fields are oscillatory; for $P_R < 1$ the amplitude and oscillations are more clearly defined.

Sequence 12

The erratic nature of two-phase interfaces leads one to believe that choking is a result of nonequilibrium nonsteady transition from liquid to vapor.

Sequence 13

Motion pictures at 16 200 frames/sec reveal that bubbles are elongated and sucked through the gap in a radial manner. The leader appears spherical and nonsteady. Higher frame rates are necessary to study the choked interface.

Sequence 14

A wide variety of flow regimes (subcooled, saturated, separated, mist, and transitions between these regimes) were illustrated as the liquid level dropped.

CONCLUSIONS

The quantitative study undertaken to determine some of the problems associated with discharging pressurized cryogens through a radial gap has revealed that:

1. Steady radial inward critical mass flow rates appear equivalent to critical mass flow rates through axisymmetric nozzles.

2. The radial flow of two-phase and supercritical mixtures through a narrow gap is not uniform. For subcooled flows the surface area covered by single phase fluid is much greater than that covered by the two-phase discharge. As subcooling diminishes the two-phase area approaches the single phase area. Over a broad range in quality (including the near critical region), the basic flow patterns are made of radial jet streams which may occupy a segment of the radial gap-nozzle or the whole gap area. Flow maldistribution is quite common and oscillations in circumferential and radial direction are obvious.

3. The critical mass flow rate data for the transient case appear different from those for the steady case. On the mass flow rate as a function of pressure map the slope and separation of isotherms for transient radial choked flow appear to be less than for steady radial choked flow. Further work and quantitative data are required to resolve the disparities between steady and transient critical radial inward flows.

REFERENCES

1. Henry, Robert E.; and Fauske, Hans K.: The Two-Phase Critical Flow of One-Component Mixtures in Nozzles, Orifices, and Short Tubes. J. Heat Transfer, vol. 93, no. 2, May 1971, pp. 179-187.

2. Smith, R. V.: Choking Two-Phase Flow Literature Summary and Idealized Design Solutions for Hydrogen, Nitrogen, Oxygen, and Refrigerants 12 and 11. Tech. Note 179, National Bureau of Standards, Aug. 3, 1963.

3. Hendricks, R. C.; Simoneau, R. J.; and Ehlers, R. C.: Choked Flow of Fluid Nitrogen with Emphasis on the Thermodynamic Critical Region. NASA TM X-68107, 1972.

4. Hendricks, Robert C.; and Simoneau, Robert J.: Application of the Principle of Corresponding States to Two-Phase Choked Flow. NASA TM X-68193, 1973.

5. Hendricks, R. C.; Baron, A.; Peller, I.; and Pew, K. J.: GASP--A Computer Code for Calculating the Thermodynamic and Transport Properties for Eight Fluids--Helium, Methane, Neon, Nitrogen, Carbon Monoxide, Oxygen, Argon, Carbon Dioxide. Presented at the 13th International Congress of Refrigeration, NAS/NRC, Washington, D. C., Aug. 27-Sept. 3, 1971.

APPENDIX-TRANSIENT RESULTS

The reservoir temperature (lower thermometer of fig. 1) pressure and thermocouple rake were monitored on strip charts. To record data, the reservoir was filled and pressurized; the recorders started, and an electronic timing mark placed on each chart; the exit valve was then opened. At low reduced pressures, a loud "crack" signaled the onset of flow out of the vent stack. The liquid level could be monitored visually (even for $P > P_c$) and the run was terminated when the liquid-gas interface reached the lower part of the glass, see figure 1.

The thermocouple rake was calibrated using 1-1-1 trichloroethane and observing the merging of the refracted and reflected images of the wire while metering the expelled liquid. With this volumetric calibration, and the response of the thermocouple rake, the fluid volume (V) exhausted as a function of time (τ) was determined. Evaporation of the liquid off the thermocouple wire as the liquid vapor interface passed usually gave a sharply defined constant time temperature trace from which one could determine the dewar level variation with time, see figure 5. Either the onset or termination of evaporation liquid and gas indicators respectively could be used to determine the volume (V) vs time curves; generally, the onset of evaporation (liquid indicator) was used. A typical series of dewar volume vs time curves are given in figure 6. Although the data do not always indicate a linear relation between V and τ, the uncertainties did not merit the use of a higher degree curve. It appears that for a given

$$(P_o, T_o),\ \frac{dV}{d\tau} = \text{constant},$$

gives a nearly accurate description of the volumetric change in the dewar.

From the experimental data

$$(P_o, T_o, \frac{dV}{d\tau}, A),$$

values for the transient critical mass flow rates can be calculated and compared with those for the steady flow case. If the critical mass flow rate is expressed as

$$G_R = \frac{G}{G^*} = \frac{(-dM/d\tau)/A(\tau)}{G^*}\Big|_{max} \qquad (1)$$

where $M = \rho V$, the mass of fluid remaining in the reservoir and $A(\tau)$ is the area of the choking front one can see immediately some of the problems in interpreting the data. Even though the rate of change of volume was reasonably constant, the average density of the fluid is difficult to determine because the pressure and temperature change with time, and temperature also may change in space. A value for the average density was calculated assuming that the temperature-time profile also represented the temperature-space profile.

$$\bar{\rho}(\tau) = \frac{1}{y_{pt} - y} \int_{y}^{y_{pt}} \rho(P,\tau)\,dy \equiv \frac{1}{\tau_{pt} - \tau} \int_{\tau}^{\tau_{pt}} \rho(\tau)\,d\tau \qquad (2)$$

The density corresponding to the stagnation pressure and assumed temperature was found using a generalized thermophysical properties program GASP (ref. 5). Typical histories for reduced stagnation pressure and temperature are given in figure 7. Note that this procedure assumes the bulk fluid to be in equilibrium, i.e. density uniquely determined by the instantaneous values of pressure and temperature in the bulk; an assumption not necessarily valid in the transient case. Finally, the actual location and area of the choking front cannot be instantaneously determined. Consequently the absolute values for transient critical mass flow rate cannot be defended. They do provide the basis for the comparison with the steady flow case, where again the actual choking front area had to be assumed. The value used for A was based on the inner diameter and passage height.

A typical variation of $G/G^* = G_R$ with time is illustrated on figure 7. Values of $G/G^* = G_R$ along selected isotherms are shown on figure 8, as a function of reduced pressure. One must note that these profiles (isotherms) appear to be nearly independent of changes with T_R, while the isotherms of figure 3 show definite changes with T_R. Furthermore, the slope of these isotherms ($\Delta G_R/\Delta P_R$) is considerably less than for the steady-state case, figure 3.

An even simpler approximation to the transient reduced critical flow rate is shown in figure 9. Here the fluid density at any time is simply taken to be that calculated from the stagnation pressure and temperature, $T_o(\tau)$ and $P_o(\tau)$, rather than attempting to correct for spatial variations through the fluid volume.

$$G_R = \frac{G}{G^*} = \frac{\rho_o(\tau)\ \frac{dV}{d\tau}}{G^*} \qquad (3)$$

A typical variation of equation (3) with time is given in figure 7. While the slopes of the isotherms on figures 8 and 9 are nearly the same, the level change between isotherms is much greater. In figure 10, a comparison is made between the steady results, figure 3, and the transient results, figure 9, for reduced temperatures of 0.8 and 0.9. Deviations in both slope and levels are to be noted.

The discrepancies may arise from the diagnostic limitations of the present, basically qualitative experiment. They may on the other hand stem from phenomena associated with the transient condition--such as nonequilibrium density in the fluid, or rapid changes in location and area of the choking front. In either case, further experimentation with more elaborate apparatus is needed to resolve the question.

The transient data obtained in this investigation are presented in table II.

TABLE I.-RADIAL INWARD CRITICAL FLOW
STEADY STATE DATA

Run	P_R	T_R	G_R
407	0.603	2.24	0.0909
408	.603	2.24	.0913
409	1.202	.705	[a]1.18
410	1.022	.706	1.056
411	.816	.708	.907
412	.606	.712	.766
413	.426	.717	.615
414	.255	.718	.377
415	.251	.719	.391
416	1.218	.793	1.107
417	1.032	.793	.942
418	.818	.798	.814
419	.611	.799	.666
420	.411	.805	.423
421	.248	.804	.0342
423	1.206	.918	.818
424	1.019	.898	.729
425	.815	.900	.603
426	.59	.902	.391
427	.572	.900	.140
428	.556	.891	[a] .062
429	.485	.891	.058
430	.599	2.05	.0907
431	.599	2.05	.0904
432	1.218	.867	.950
433	.985	.869	.800
434	.794	.870	.659
435	.592	.874	.475
436	.592	.872	.475
437	.445	.877	.0945
438	1.190	.988	.568
439	1.121	.967	.589
440	1.117	.966	.5895
441	1.034	.965	.523
442	.995	.965	.489
443	.958	.966	.459

[a]Questionable.

TABLE I.-CONCLUDED.-RADIAL INWARD CRITICAL FLOW STEADY STATE DATA

Run	P_R	T_R	G_R
444	0.878	0.970	0.192
445	1.266	.975	[a] .76
446	1.267	1.044	.314
447	1.267	1.042	.314
448	1.205	1.032	.291
449	1.128	1.023	.262
450	1.052	1.011	.236
451	1.025	1.007	.226
452	.927	.990	.190
453	.844	.975	.163
454	.646	.934	.101

[a]Questionable.

TABLE II.-TRANSIENT RADIAL INWARD CRITICAL FLOW
DATA INTERPOLATED TO SELECTED ISOTHERMS

$T_R = 0.7$					$T_R = 0.75$					$T_R = 0.8$				
P_R	ρ_R	$\Delta V/\Delta\tau$	G_{R_1}	G_{R_2}	P_R	ρ_R	$\Delta V/\Delta\tau$	G_{R_1}	G_{R_2}	P_R	ρ_R	$\Delta V/\Delta\tau$	G_{R_1}	G_{R_2}
0.2	2.42	59.5	0.62	0.49	0.29	2.32	68.2	0.57	0.54	0.39	2.2	88.6	0.69	0.68
.22	2.42	66.9	.55	.55	.39	2.32	73.3	.63	.58	.47	2.2	87.8	.75	.66
.31	2.42	68.2	.53	.56	.39	2.33	88.6	.72	.7	.55	2.2	92.6	.77	.69
.39	2.42	73.3	.67	.61	.48	2.33	87.5	.74	.69	.56	2.2	93.7	.76	.66
.39	2.43	88.6	.735	.73	.56	2.33	82.6	.77	.73	.65	2.22	97.9	.8	.74
.49	2.43	87.8	.77	.73	.58	2.33	93.7	.79	.6	.73	2.24	105.4	.97	.8
.58	2.43	92.6	.8	.77	.65	2.33	97.9	.8	.78	.74	2.2	98.2	.8	.73
.59	2.43	93.7	.83	.77	.74	2.34	105.4	.96	.84	.83	2.23	105.3	.86	.8
.71	2.44	97.9	.82	.81	.75	2.33	98.2	.82	.78	.83	2.24	109.7	.94	.83
.75	2.44	105.4	.93	.88	.84	2.35	105.3	.9	.84	.89	2.2	114.8	1.0	.87
.78	2.44	98.2	.82	.82	.85	2.34	109.7	.9	.87	.91	2.24	110.1	.92	.84
.86	2.45	109.7	.96	.92	.89	2.34	114.8	1.03	.92	.94	2.22	111.5	1.01	.86
.88	2.45	105.3	.87	.88	.92	2.35	110.1	.94	.88	.96	2.24	121.6	1.0	.92
.91	2.45	114.8	.98	.95	.95	2.35	111.5	.97	.89	.98	2.24	115.2	.95	.88
.98	2.45	115.2	.99	.92	.97	2.35	121.6	.99	.97	1.01	2.25	122.4	1.07	.94
1.03	2.45	121.6	1.03	1.015	.99	2.35	115.2	.97	.92	1.03	2.25	128.2	1.06	.98
1.06	2.45	115.2	.93	.96	1.04	2.35	122.4	1.01	.98	1.04	2.24	119.6	1.06	.91
1.09	2.45	122.4	1.06	1.02	1.06	2.35	119.6	1.03	.96					
1.1	2.45	119.6	1.03	1.0	1.06	2.35	128.2	1.07	1.02					

TABLE II.-CONCLUDED.-TRANSIENT RADIAL INWARD CRITICAL FLOW DATA INTERPOLATED TO SELECTED ISOTHERMS

$T_R = 0.85$					$T_R = 0.9$				
P_R	ρ_R	$\Delta V/\Delta\tau$	G_{R_1}	G_{R_2}	P_R	ρ_R	$\Delta V/\Delta\tau$	G_{R_1}	G_{R_2}
0.56	2.08	93.7	0.8	0.68	0.73	1.9	98.2	0.83	0.63
.65	2.08	97.9	.8	.69	.81	1.91	109.7	.91	.73
.73	2.09	98.2	.83	.7	.82	1.9	105.3	.89	.68
.73	2.1	105.4	1.05	.77	.88	1.91	114.8	.97	.76
.82	2.09	105.3	.86	.75	.9	1.95	110.1	.92	.73
.82	2.1	109.7	.94	.78	.93	1.95	121.6	.93	.82
.88	2.1	114.8	1.0	.82	.96	1.94	115.2	.95	.76
.92	2.1	111.5	1.03	.82	.99	1.94	122.4	1.1	.81
.95	2.1	121.6	.96	.87	1.0	1.95	128.2	1.02	.85
.96	2.12	115.2	.95	.83	1.02	1.95	119.6	1.09	.79
1.0	2.1	122.4	1.1	.87					
1.02	2.1	128.2	1.05	.91					
1.03	2.12	119.6	1.06	.86					

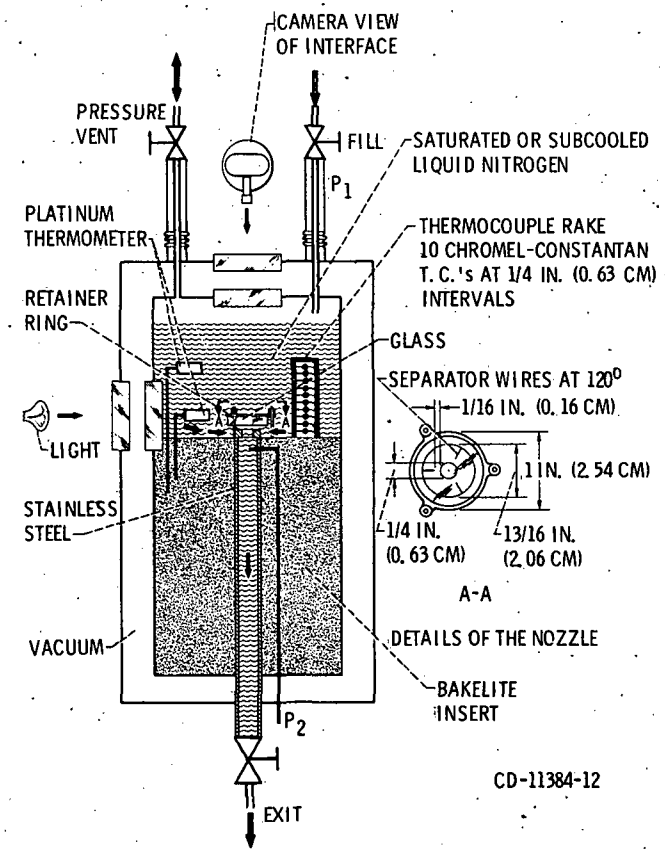

CS-67134 Figure 1. - Visualization of flow of LN_2 into radial gap.

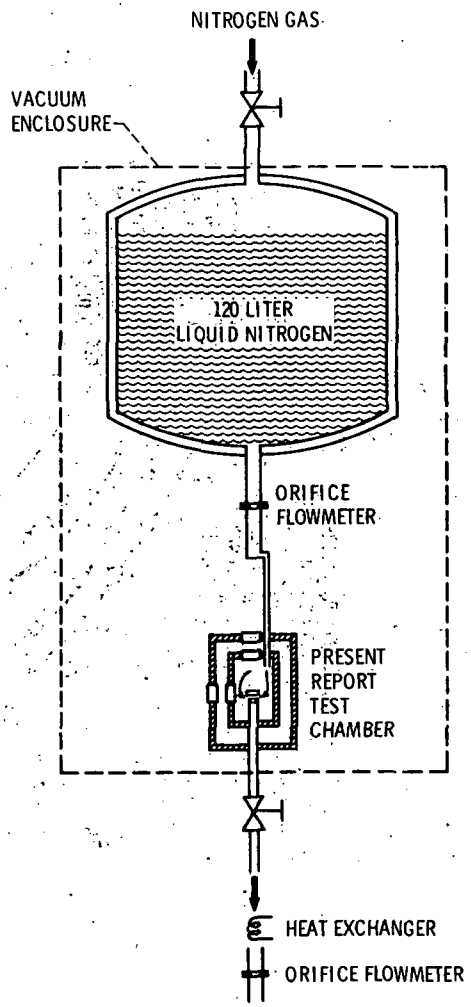

Figure 2. CS-67136

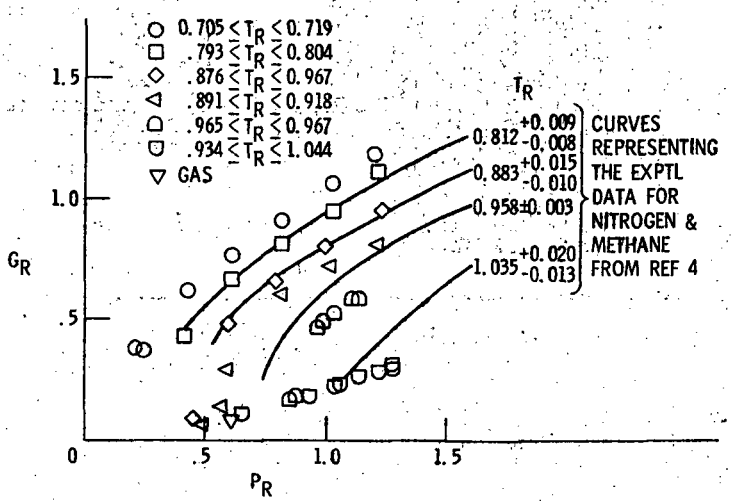

Figure 3. - Steady state radial inward critical flow as a function of reduced pressure for selected "isotherms."

CS-67131

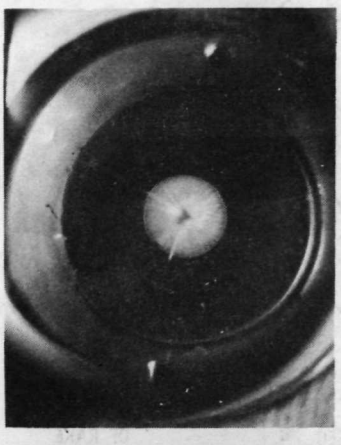

(a) REPRESENTS FILM SEQUENCE 1.

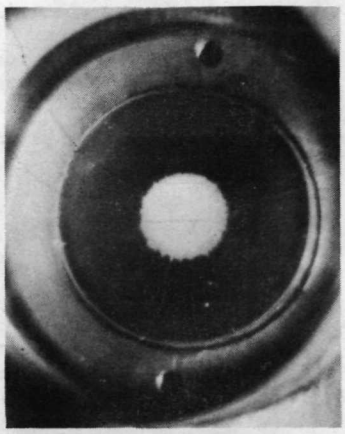

(b) REPRESENTS FILM SEQUENCE 2.

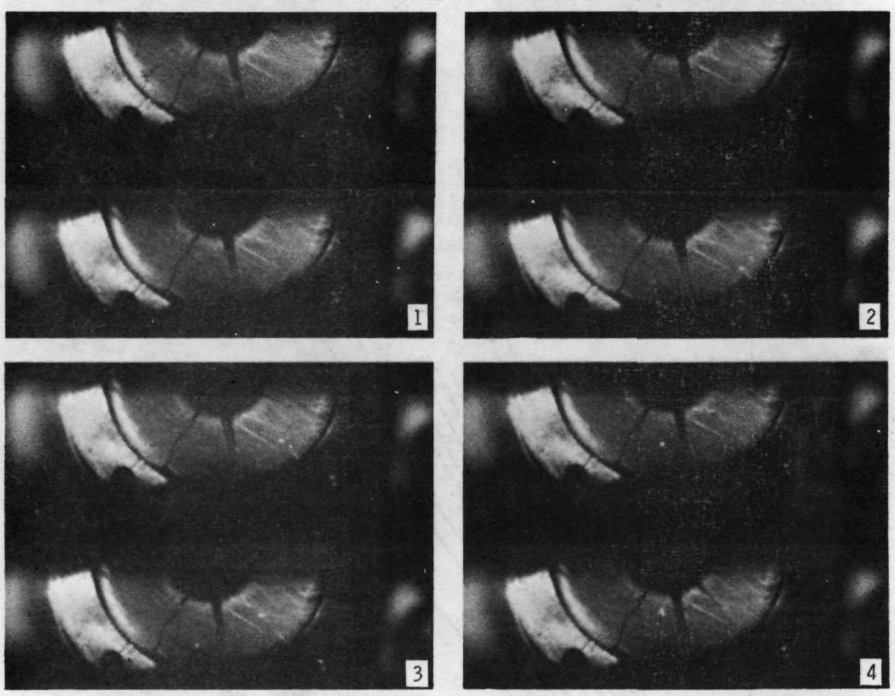

(c) REPRESENTS FILM SEQUENCE 9.

Figure 4. - Photographs which represent selected film sequences of the accompanying motion picture.

CS-67126

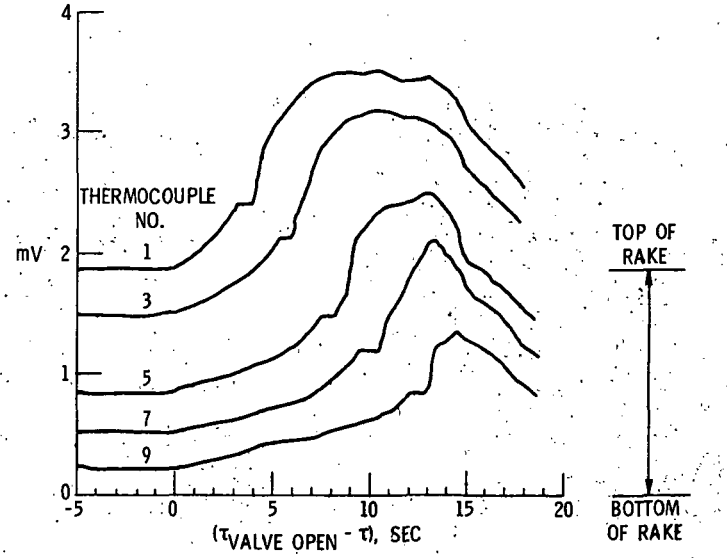

Figure 5. - Typical time temperature profiles of the thermocouple rake. CS-67132

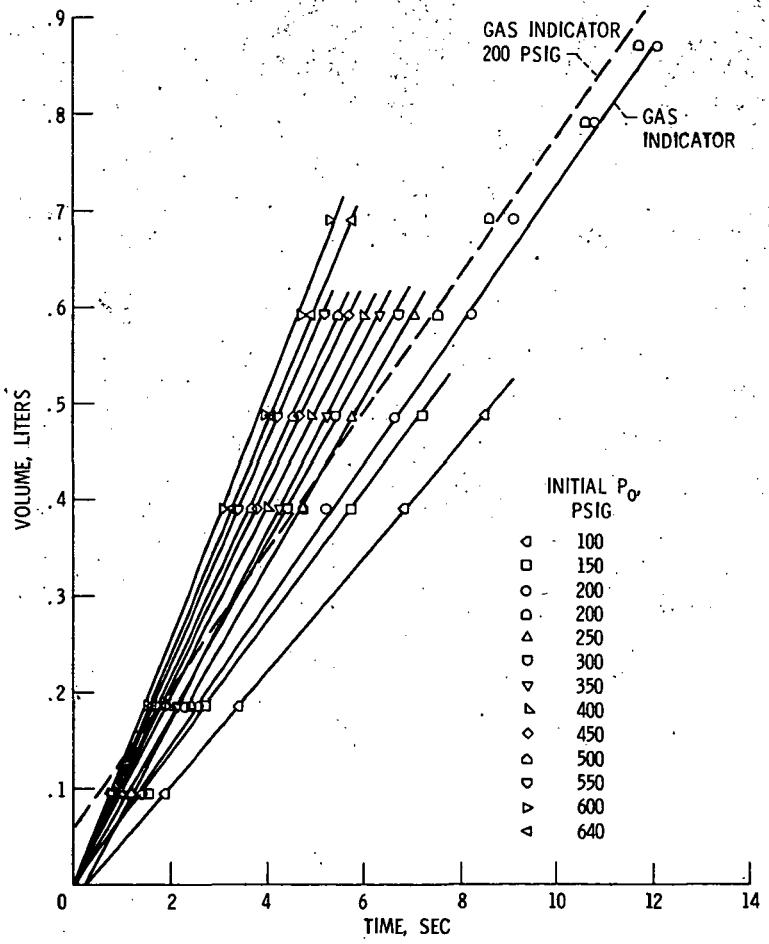

Figure 6. - Variation of dewar volume as a function of time for several initial pressure levels. CS-67135

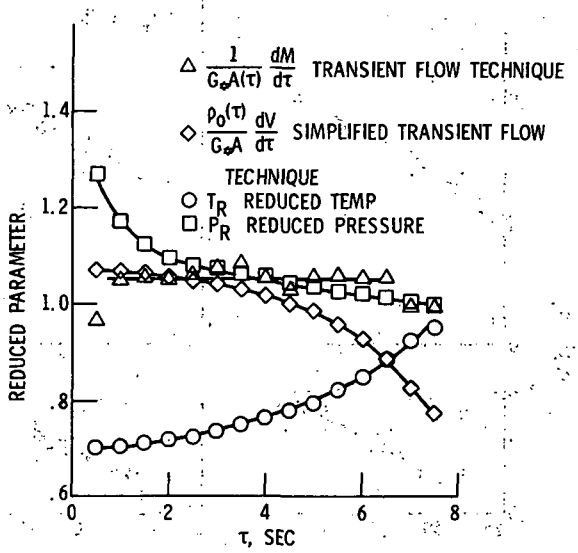

Figure 7. - Variation of parameters with time for an initial stagnation pressure of 600 psig. CS-67130

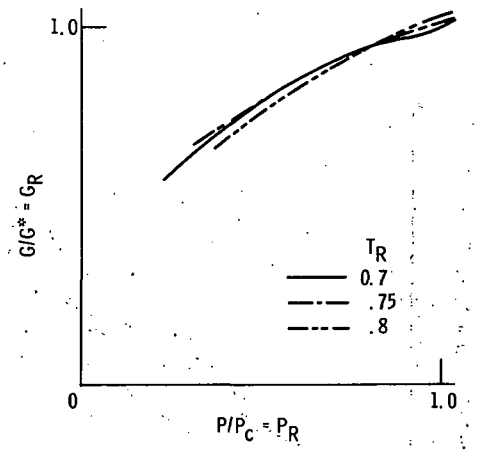

Figure 8. - Transient radial inward flow data based on $G = \left(\frac{dM}{d\tau}\right) / A(\tau)$. CS-67129

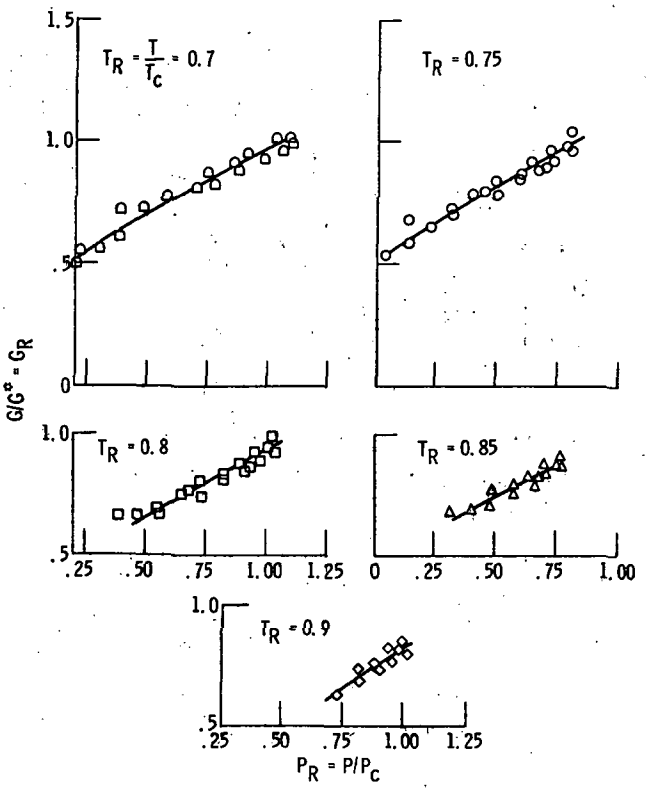

Figure 9(a). - Transient radial inward critical flow for selected isotherms based on $G = \rho(dV/d\tau)/A$.

CS-67133

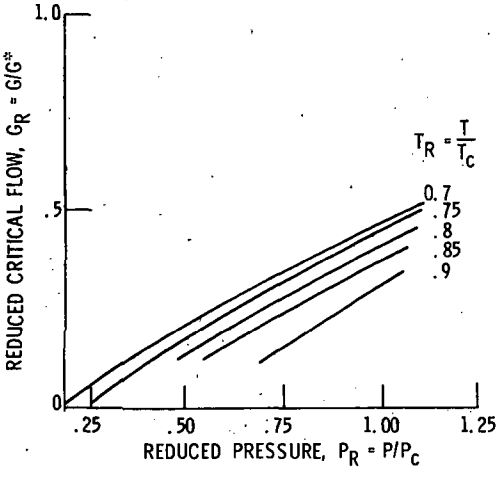

Figure 9(b). - Transient radial inward flow for selected isotherms - smoothed results.

CS-67128

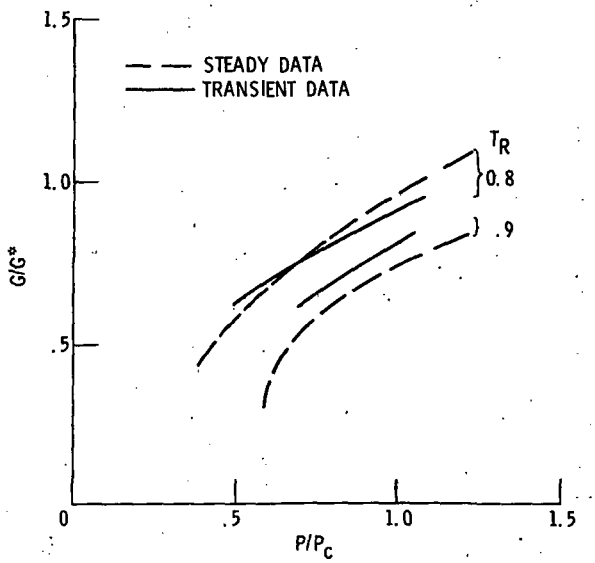

Figure 10. - Comparison of transient and steady reduced critical flow rates for selected isotherms.

CS-67127

Page Intentionally Left Blank